Validation of an unstructured CFD solver for complete helicopter configurations with loose CSD-Trim coupling

Jan-Hendrik Wendisch and Jochen Raddatz

German Aerospace Center
Institute of Aerodynamics and Flow Technology
Lilienthalplatz 7, 38108, Braunschweig, Germany
jan-hendrik.wendisch@dlr.de;jochen.raddatz@dlr.de

The present study addresses the applicability of the unstructured CFD solver TAU of the German Aerospace Center (DLR) for the simulation of isolated rotors and complete helicopter configurations. Rotor trim and elasticity of the rotorblades is taken into account by loose fluid-structure-trim coupling. Numerical results are presented and compared to experimental measurements of the GOAHEAD windtunnel campaign. The selected testcase of the GOAHEAD experimental database corresponds to a cruise flight condition at Ma=0.204 with an advance-ratio of $\mu = 0.33$. Validation results for the isolated mainrotor are in excellent agreement with CFD reference solutions and in good agreement with experimental data. CFD simulation for the rotor-fuselage configuration shows a good correlation with experimental data.

Abbreviations

AH	Airbus Helicopters
BDF	Backward Differentiation Formula
CFD	Computational Fluid Dynamics
CSD	Computational Structural Design
DLR	Deutsches Zentrum für Luft- und Raumfahrt
DNW	Deutsch-Niederländische Windkanäle
FMC	Fourier mode Shape Coefficients
GCL	Geometric Conservation Law
GOAHEAD	Generation of Advanced Helicopter Experimental Aerodynamic Database
HOST	Helicopter Overall Simulation Tool
LLF	Large Low-speed Facility
RANS	Reynolds-Averaged Navier-Stokes
SPA	Strain-Pattern-Analysis
SPR	Stereo-Pattern-Recognition

1 Introduction

Today Computational Fluid Dynamics (CFD) has become a reliable prediction tool and is succesfully applied for complete helicopter configurations[2]. Structured CFD solvers are well established and validated for helicopter simulations while the utilization of their unstructured counterparts is often merely limited to the simulation of isolated helicopter components like the main rotor or the bare fuselage. Unstructured methods are favorable in terms of grid dimension and time consumption for the grid generation process for highly detailed and complex geometries. The grids can easily refined locally allowing high spatial resolution of flow phenomena in areas of interest.

For validation of CFD-codes for helicopter applications the EU-Project GOAHEAD[14] was launched in 2005. In a windtunnel campaign at the German-Dutch Windtunnel (DNW) a complete helicopter configuration was measured for several flight and rotor loading condtions. Based on the windtunnel experiment a database including steady and unsteady surface pressures on the fuselage, rotors, flow field velocity measurements, transition locations, blade dynamics was created. To avoid differences in the geometry representation between experiment and simulation the windtunnel geometry was digitized by laser measurements after the windtunnel tests.

The blades of a helicopter rotor are thin and their elastic deformation on a loaded rotor has a considerable influence of the rotor performance. Torsional bending, lead-lag and flap deflection of the blade modify the local inflow direction at the blade leading to differences in the performance compared to rigid blade assumption[10]. These effects become quite large if stiffness of the blades decreases or the load of the rotor is increased. For accurate prediction of the performance of helicopter rotors by CFD computations the dynamic behaviour of the blade and its elastic deformation is taken into account by coupling the flowsolver to a flight and structural mechanic tool.

The applied numerical methods are shortly introduced in section 2, while the studied helicopter configuration and the flow conditions are described in section 3. Verification and validation of the unstructured flow solver is described in detail in section 4 and conclusion is drawn in section 5.

2 Numerical methods

The numerical results of the present work are based on time-accurate solution of the Reynolds-Averaged Navier-Stokes (RANS) equations. Time-integration of the RANS equations is done via second order Backward Differentiation Formula (BDF2) according to[9]. At DLR the second-order accurate unstructure flow solver TAU[18] is currently validated for simulations of isolated rotors and complete helicopter configurations. The solver is equipped with a large variety of turbulence models ranging from one-equation eddy viscosity models[17] to more sophisticated seven-equation Reynolds-Stress models[13]. Relative movement of the rotorblades is realized by the Chimera technique[8,19] and the spatial discretization of the solver accounts for moving and deforming meshes satisfying the geometric conservation law[7]. Numerical reference solutions considered in this work are provided by DLRs well-validated blockstructured flow solver FLOWer[12].

2.1 Fluid-structure-trim coupling

To incorporate elastic deformation of the rotor blades and the related control angles to trim the rotor in the simulation the flow solver needs to be coupled to an external comprehensive rotorcode providing the necessary data. The coupling module implemented in FLOWer is described in detail in[4]. In case of TAU a new coupling tool has been developed at DLR allowing to loosely couple the solver to different comprehensive rotorcodes and is in principle not limited to TAU on the CFD-side. The exchange of data during the simulation is performed within memory whenever possible significantly reducing file I/O operations in both cases.

Throughout this paper the structural deformation and the trim angles are provided by the comprehensive rotorocode *Helicopter Overall Simulation Tool* (HOST)[1] of *Airbus Helicopters* (AH). A pure force trim is applied meaning that the integral averaged propulsive force, side-force and lift are set

as trim objectives for the rotor. The loose fluid-structure-trim coupling process can be briefly summarized in five steps:

1. At the beginning of the fluid-structure-trim simulation HOST computes the inertial rotor trim based on its own simplified aerodynamic. Besides the trim angles HOST provides the complete dynamic of the rotorblade as modal base data and generalized coordinates.

2. From the modal base data and the generalized coordinates the azimuth dependent deformation of the blades is reconstructed. The deformations are propagated into the computational grid and a CFD simulation of one physical timestep is performed.

3. From the CFD simulation sectional lineloads respectivily line moments on the rotorblade quarterchord line are computed at discrete radial positions and transferred into HOSTs reference frame.

4. The steps 2 and 3 are repeated unitl a periodical flow state is achieved and loads for one rotor revolution can be provided to HOST. The sectional loads $F_{CFD}(\Psi)$ from the CFD simulation are now used to correct the sectional loads F_{2D} of HOST:

$$F^n_{HOST}(\Psi) = F^n_{2D}(\Psi) + F^{n-1}_{CFD}(\Psi) - F^{n-1}_{2D}(\Psi) \quad (1)$$

   with n denoting the n-th coupling cycle. Based on the corrected sectional loads the trim angles and generalized coordinates are recomputed.

5. The steps 3 to 4 are repeated until HOSTs internal aerodynamic is completely replaced by the aerodynamics of the CFD simulation. Thus, the simulation is converged if the difference

$$\Delta F^n(\Psi) = F^n_{2D}(\Psi) - F^{n-1}_{2D}(\Psi) \quad (2)$$

   approaches zero. In case of a converged simulation the aerodynamic of HOST and CFD are identical:

$$F_{HOST}(\Psi) = F_{CFD}(\Psi) \quad (3)$$

A detailed description of the trim process and the reconstruction of the deformed blade surface based on the output of HOST can be found in[5,11].

The main difference between the used FLOWer-HOST and TAU-HOST coupling tool chains used in the present study originates from the unstructured approach of TAU. In step 3 the aerodynamic loads of the CFD surface mesh needs to be transferred to the beam model used in HOST. This is generally achieved in structured flowsolvers by summing up the loads along gridlines. Since TAU can use mixed-element meshes composed of triangles and quadriliterals for the surface discretization a different, more general approach is used. Instead of directly using the CFD surface mesh an auxiliary mesh is introduced. The surface loads from the CFD computation are transferred onto this mesh by an energy-preserving interpolation scheme based on radial basis functions. For the coupling of TAU to comprehensive rotorcodes a structured quadriliteral mesh is used comparable to a surface blade mesh of a structured flowsolver. The computation of the loads on the beam model can then performed analogous to the FLOWer-HOST coupling. Additionally this approach allows the transfer of loads from the CFD to arbitrary Finite-Element meshes enabling the coupling tool to provide data for Finite-Element codes in order to replace HOST by more accurate FEM-solvers in the future.

3 Experimental Setup

In the european GOAHEAD project a 1:3.88 scaled complete helicopter configuration was measured in the 6 mx8 m test section of the Large Low-speed Facility (LLF) at the German-Dutch windtunnels[14]. The configuration is composed of a four-bladed ONERA 7AD mainrotor, a two-bladed BO105 tailrotor, a rotor hub and a fuselage including control surfaces comparable to a NH90. Experimental data of 300 steady pressure taps, 130 unsteady pressure taps, hotfilms and microtufts for the 4.1 meter long fuselage is available. The 2.1 meter long blades of the clockwise rotating rotor (seen from above) are equipped with pressure transducers at different span-wise positions and hotfilms. In total 118 pressure sensors can be used for comparison of the pressure distributions of the mainrotor blades. Movement of the rotorblades was optically measured by using Stero-Pattern-Recognition (SPR)[15] complementary to Strain-Pattern-Analysis (SPA) of strain-gauges integrated in one dedicated blade. For a detailed description of the windtunnel experiment the reader is referred to[14].

From the different testcases of the GOAHEAD campaign the cruise testcase is used as reference for the verification and validation of the unstructured flow solver TAU for fluid-structure-coupled simulations. The selected testcase corresponds to an inflow Mach-number of 0.204 and an advance ratio of $\mu = 0.33$ resulting from an angular velocity of $\omega = 951 min^{-1}$ of the mainrotor.

4 Results

4.1 Isolated GOAHEAD 7AD Mainrotor

In order to carefully validate the new coupling interface for TAU the isolated GOAHEAD rotor is simulated first. To eliminate grid induced differences in the flow solution the identical mesh as depicted in figure 1 is used for the TAU simulation and the FLOWer simulation. The mesh is a pure hexahedral mesh consisting of four blade meshes with 0.81 million points each and the background mesh with 2.91 million points. For the simulations the Wilcox k-ω turbulence

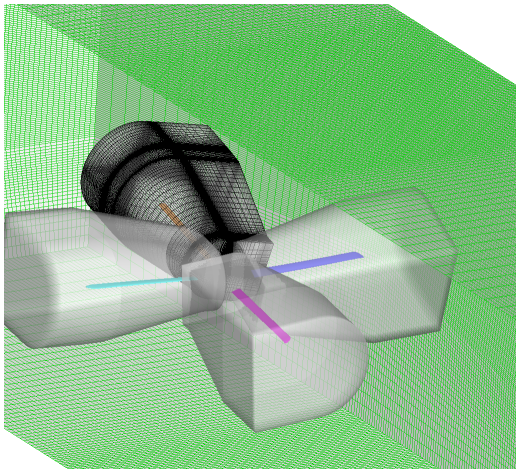

Figure 1: Hexahedral mesh of isolated 7AD mainrotor

model of[3] and a timestep corresponding to one degree of mainrotor azimuthal increment is used. The timesteps in pseudo-time of the dual-time stepping scheme are stopped if the forces and moments converge to a constant value. In the FLOWer simulation this leads to a reduction of the residual by four orders of magnitude and five orders by magnitude in the TAU simulations.

4.1.1 Convergence of the control angles

The convergence of the iterative determination of the control angles is depicted in figure 2. Within the coupled simulations three rotor revolutions are performed for the first trim iteration. All successive trim iterations are performed after one additional rotor revolution. The iteratations are repeated until the incremental change in all trim angles drops below a threshold of $1e^{-03}$ degree. Both coupling chains converge after the seventh trim iteration. Among the numerical simulations the difference in the trim angles is very with a maximum deviation of 0.04 degree in the longitudinal control angle Θ_s.

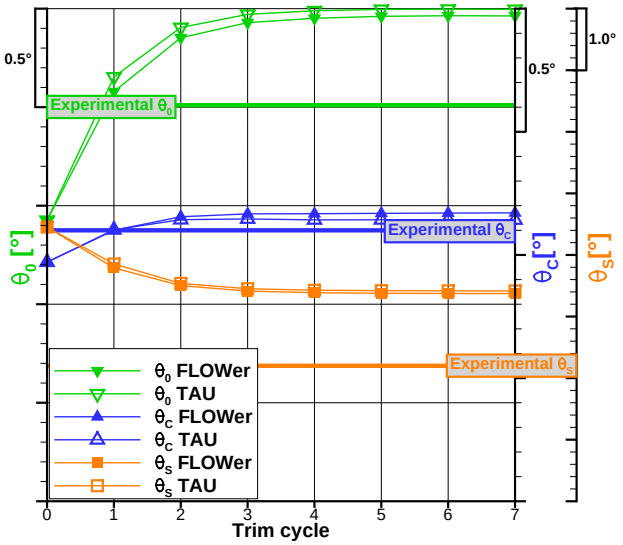

Figure 2: Convergence of the computed control angles in comparison to the measurement for the 7AD mainrotor testcase. Hollow symbols: TAU simulation. Filled symbols: FLOWer simulation

Experimental control angles can not completely matched since the simulation is limited to an isolated rotor neglecting all interference effects with the fuselage. Nevertheless the collective Θ_0 and lateral control Θ_C are in good agreement with the experiment. The deviations are below 0.5 degree for the collective control respectively 0.07 degree for the lateral control. Simplification of the simulation seem to mainly affect prediction of the longitudinal control angle leading to an offset of roughly 1.3 degree. Based on the observation it can be stated that the lateral-force between simulation and experiment differs since the longitudinal control has to compensate the lateral-force to fulfill the trim goal.

4.1.2 Global loads

Due to contractual obligations the global loads of figure 3 are plotted in normalized form with arbitrary reference values (note: the scales in the plots are very small). Experimental data of the mainrotor balance was corrected during the measurements to approximately giving the net loads of the isolated rotor blades without the loads on the rotorhub.

The shown numerial results of the TAU and FLOWer computation are in excellent agreement among each other both in amplitude and phase. Numerical results will unlikely match the experimental values because of the neglected interference effects. For judgement of the data the mean values denoted as dashed lines are added to the figures. The

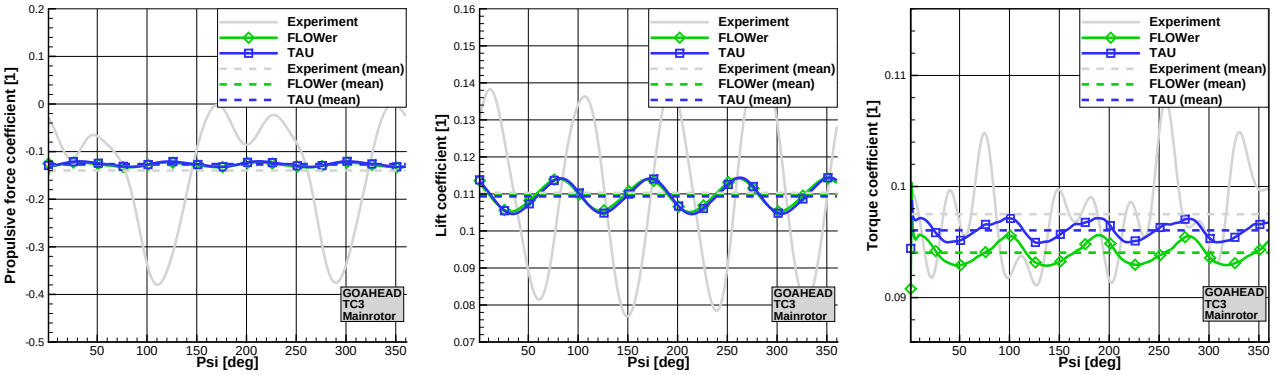

(a) Mainrotor propulsive coefficient (b) Mainrotor lift coefficient (c) Mainrotor torque coefficient

Figure 3: Normalized force and moment coefficients for the mainrotor for the 7AD mainrotor testcase. Blue curve: TAU. Green curve: FLOWer. Grey curve: Experiement. Dashed lines denote mean values

mean values for the main rotor propulsive and lift forces differ slightly, because the nominal trim objective was not exactly matched in the wind tunnel experiment, whereas the trim objective is exactly fulfilled by the CFD simulations.

The measured propulsive force exhibits a pronounced 2/rev peak occuring at 110 degree and 290 mainrotor azimuth (s. fig. 3a) which is not present in the simulation. The origin of the unexpected 2/rev signal in the experimental data is unknown. Experimental mainrotor lift (s. fig. 3b) is dominated by a periodic 4/rev signal. Its Amplitude and phase can not be captured by the simulations. A clear 10/ref frequency content in the experimental mainrotor torque (s. fig. 3c) originating from the tailrotor with its characteristic frequency of 10/rev is present. Data from the mainrotorbalance could not be corrected for tailrotor loads. Because the balance is mounted in the fuselage its data is biased by the tailrotor forces acting on the fuselage leading to vibrations of the model since wether the fuselage nor the windtunnel support is ideally stiff.

4.1.3 Pressures distributions on the mainrotor

In figure 4 the computed and measured Mach-scaled pressure distributions are compared. Unsteady pressures are available at five radial positions for three rotorblades. The unsteady pressures are averaged over 150 rotor revolutions and compared at the outermost radial position of r/R = 0.975 with the numerical results of the last trim cycle. Throughout the whole revolution the results of the FLOWer-HOST and TAU-HOST coupling are in very good agreement among each other.

Despite the simplications in the simulations a rather good agreement in the measured and computed pressure distributions is achieved. The differences result from the different local inflow conditions at the blade section due to the missing interference effects of the fuselage and deviations in the blade dynamics, as will be shown in the following section.

4.1.4 Blade dynamics

In this section the computed and measured deflections near the blade tip are compared. In case of the flap and lead-lag deflection the results obtained by SPR-technique of all four rotor blades are used. The reported theoretical accuracy in x-,y- and z-direction is 0.4mm. Discrete data is available in 11.25 degree mainrotor azimuth increment at 14 radial positions. The data was used to generate a continous representation in radial and azimuth direction based on Fourier series and mode shape coefficients (FMC) which is available in the GOAHEAD database. The shown results for the flap and lead-lag deflection represent the full dynamic state of the blade including the motion about the hinges and the elasticity of the blade. For comparison of the torsion motion the SPA data is used since it provides a better harmonic content[6]. In contrast to the flap and lead-lag deflection the data only contains the pure elastic deformation without any motion about the hinges and is limited to one dedicated blade.

All simulations predict the 2/rev characteristic of the flap motion very well (s. fig. 5). Only the pure HOST computation shows a phase shift of approximately 20degree which is removed by the coupling to CFD. However CFD predicts only half of the flap deflection compared to the experiment. The deviations are mainly attributable to the neglected interference effects with the fuselage. The longitudinal control angle (s. section 4.1.1) is off by nearly 1.3 degree also affecting the flap motion.

In contrast to the flap motion the experimental determined

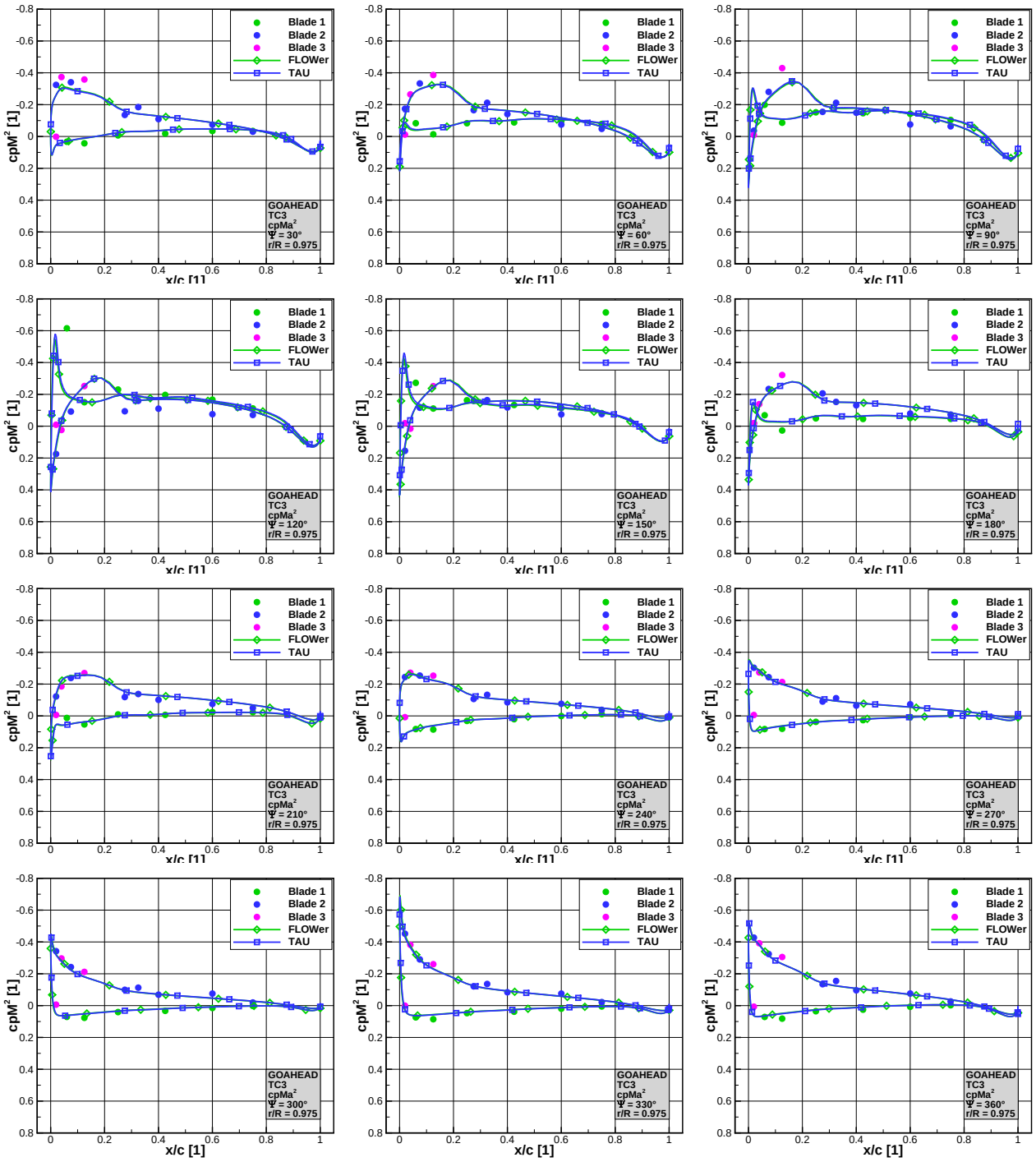

Figure 4: Computed and measured main rotor sectional pressures at r/R = 0.975 for a complete revolution for the 7AD mainrotor testcase. Green curve: FLOWer. Blue curve: TAU. Circles: Experiment. Circles of different colors denote different blades.

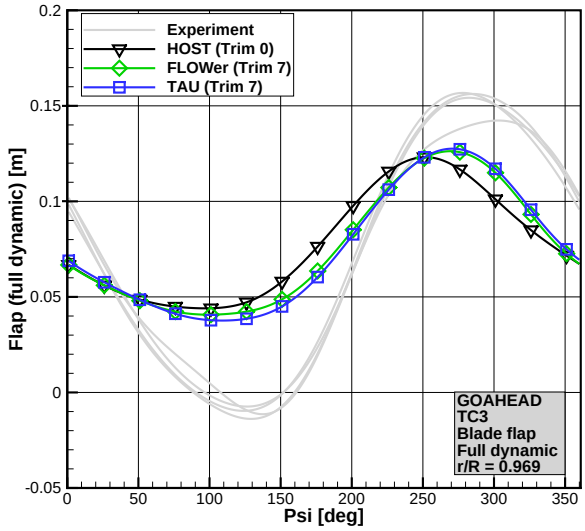

Figure 5: Computed and measured flap motion of the 7AD mainrotor testcase near the blade tip. Black curve: HOST. Green curve: FLOWer. Grey curves: SPR

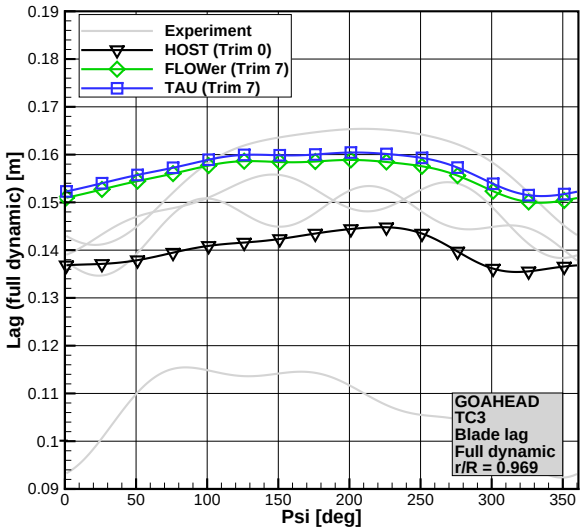

Figure 6: Computed and measured lead-lag motion of the 7AD mainrotor testcase near the blade tip. Black curve: HOST. Green curve: FLOWer. Grey curves: SPR

lead-lag motion of figure 6 shows a different dynamic behaviour of the four rotor blades. Especially the motion of one blade differs significantly (results are situated at the bottom of the figure).

The data of the measurement is consistent since the same behaviour is observable in all testcases of the GOAHEAD database. The reasons are manifold ranging from blade to blade differences (mass distribution, inertia) or differences in the lead-lag damper. Within the simulation all blades are modelled identically leading to identical dynamic behaviour of the blades. CFD increases the predicted lead-lag motion and the results are situated at the upper end of the scattering range of the experimental data.

As depicted in figure 7 the 5/rev characteristics of the torsion mode is not captured by any computation.Except for the strong 5/rev oscillation the simulations follow the trend of the experiement.There are multiple reasons for the deviations. On the one hand the disortion of the inflow due to the displacement of the fuselage has an significant impact on the torsion moment and is not present in the simulation. On the other hand the beam model in HOST may not be sufficient to predict the torsion of the rotorblade accurately enough.

From the comparison of the blade dynamics it can be concluded that the results of the TAU-HOST and FLOWer-HOST are in excellent agreement among each other with a maximum difference of 3.5 millimeters in the flap motion, 1.5 millimeters in lead-lag motion and 0.2 degree in torsion.

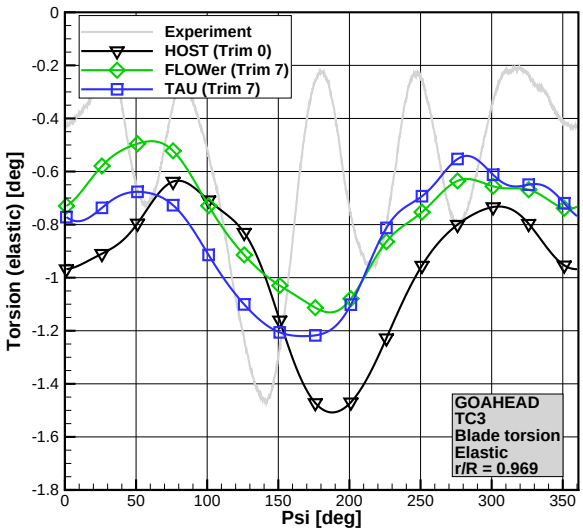

Figure 7: Computed and measured torsion motion of the 7AD mainrotor testcase near the blade tip. Black curve: HOST. Green curve: FLOWer. Grey curve: SPA

4.2 GOAHEAD configuration

For the fuselage a mixed-element mesh was created with the commercial grid generator PointWise[16]. In the mesh the wakes of the backdoor, mainrotor and the engine exhausts are locally refined. Hexahedral cells were added near the top of the fuselage allowing an easier control of the Chimera overlap of the mainrotor. In order to reduce complexity the numerical setup does not inlcude the tail rotor. The mainrotor grids from the isolated testcase were reused leading to a total of 15 million points for the simplified mesh (s. fig. 8).

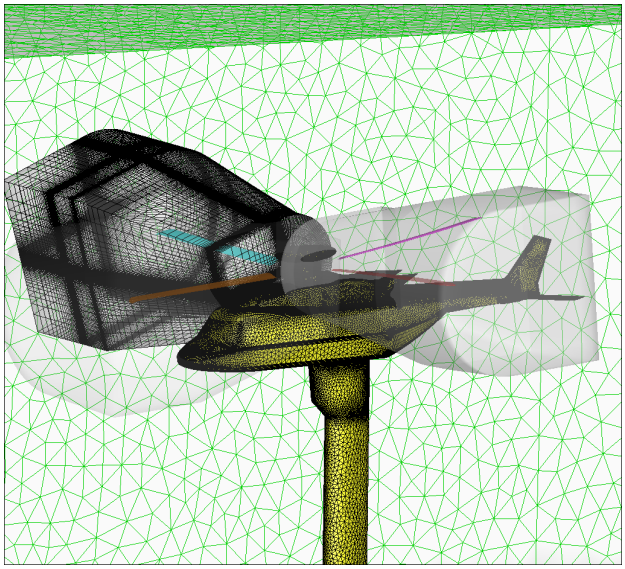

Figure 8: Mixed element mesh of simplified GOAHEAD configuration

Identical to the isolated rotor testcase the timestep corresponds to one degree of mainrotor azimuthal increment. Also the Wilcox k-ω turbulence model is used but in conjunction with a vortical flow correction. The timesteps in pseudo-time of the dual-time stepping scheme are stopped if the forces and moments converge to a constant value and the residual is at least reduced by five orders of magnitude. The computation has been performed for three rotor revolutions and two trim couplings. Additional trim iterations will be needed to reach the final trim state. Results of the subsequent sections already indicate the influence of the fuselage on the rotor dynamic.

4.2.1 Convergence of the control angles

For the simplified configuration the first trim based on CFD aerodynamics is performed after the second rotor revolution. Instead of performing a trim iteration after a complete revolution like for the isolated mainrotor all trim iterations are performed after one half of a rotor revolution. In principle exchange can be also performed after 90 degree (for a four-bladed rotor) but disturbances originating from the coupling process due to the sudden change of the trimangles and the blade deformation may negatively affect the trim computation.

The preliminary results of the control angles (s. fig. 9) are in good agreement with the isolated rotor tetcase, but influence of the fuselage is also noticeable. In comparison to the isolated rotor the simulation tends to predict a collective and longitudinal angle closer to the experimental results. But the lateral control angle tends to be overpredicted. Since the control angles are not fully converged a final conclusion can not be drawn.

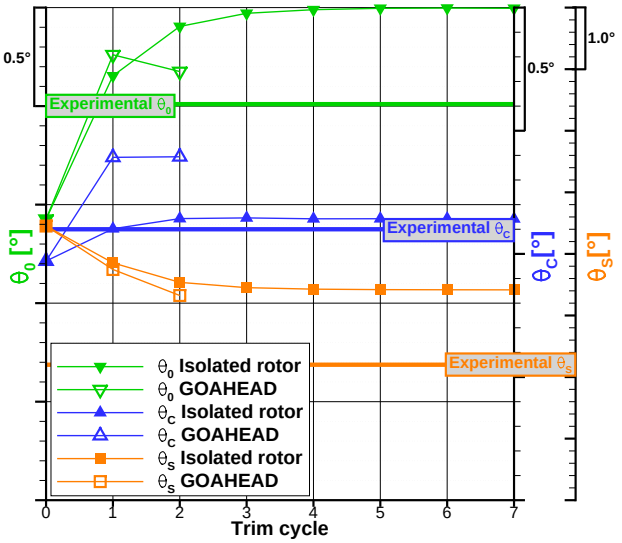

Figure 9: Convergence of the computed control angles in comparison to the measurement of the simplified GOAHEAD configuration. Filled symbols: Isolated rotor. Hollow symbols: simplified GOAHEAD configuration

4.2.2 Pressure distributions on the fuselage

The general pressure distribution on the fuselage at $\Psi = 270$ degree mainrotor azimuth is depicted in the figure 10. The spheres and octahedrons denote the experimental unsteady respectively steady pressure coefficients. The numerical pressure distribution over the whole fuselage is in good agreement with the experiment data.

At the symmetry plane the pressure distributions (11) of

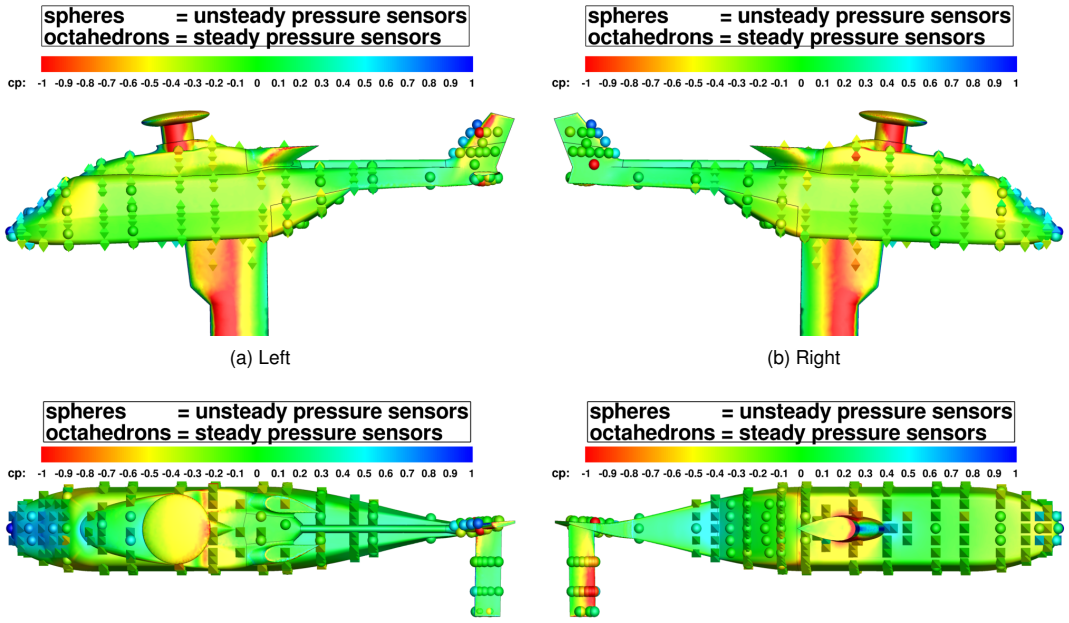

(a) Left (b) Right

(c) Top (d) Bottom

Figure 10: Comparison of computed and measured pressure distribution on the simpflied GOAHEAD configuration. Spheres: Unsteady pressure sensors. Octahedrons: Steady pressure sensors.

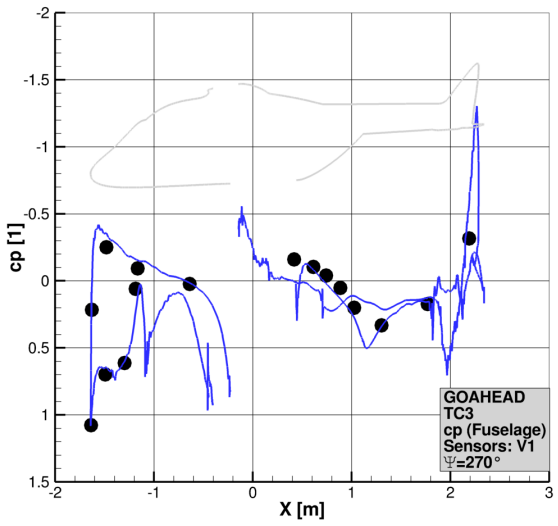

Figure 11: Comparison of computed and measured pressure distributions at fuselage symmetry plane of the simplified GOAHEAD configuration. Circles: Experiment

the simulation and the experiment is compared. Overall good agreemenent is achieved. The simulation is capable to predict the rapid pressure drop at the nose and the pressure recovery zones at the windshield and the mast fairing are accurately captured.

4.2.3 Blade dynamics

As already assumed in section 4.1.4 the predicted flap motion (s. fig. 12) is considerable improved compared to the isolated rotor testcase. The amplitude of the flap motion is increased and the results are driven closer to the maximum and minimum of the experimenal values. On the retreating blade-side a slight shift in the phase of the flap motion is present.

Comparable to the isolated rotor testcase the lead-lag deflection in figure 13 is increased by the CFD. From the preliminary results for the lead-lag deflection it can be stated that the influence of the fuselage is rather small and the shape of the lead-lag motion is not significantly altered.

Frequency content of the elastic torsion is increased in the simulation of the simplified GOAHEAD configuration (s. fig 14) and the 5/rev content of the experiment is present in the simulation. But still the amplitude is smaller and a shift in the phase exist.

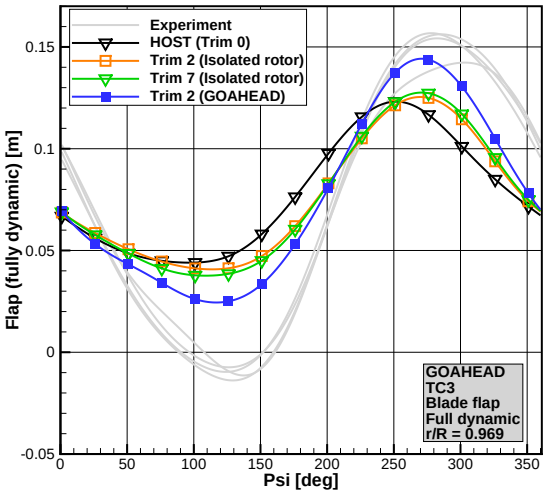

Figure 12: Computed and measured flap deflections of the simplified GOAHEAD configuration after the second trim cycle near the blade tip. Grey curves: SPR

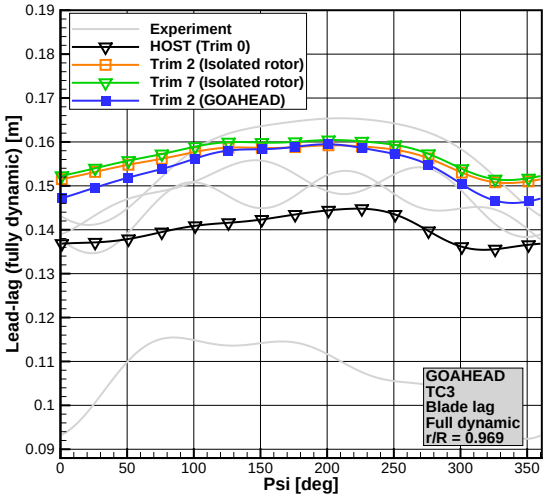

Figure 13: Computed and measured lead-lag declection of the simplified GOAHEAD configuration after the second trim cycle near the blade tip. Grey curves: SPR

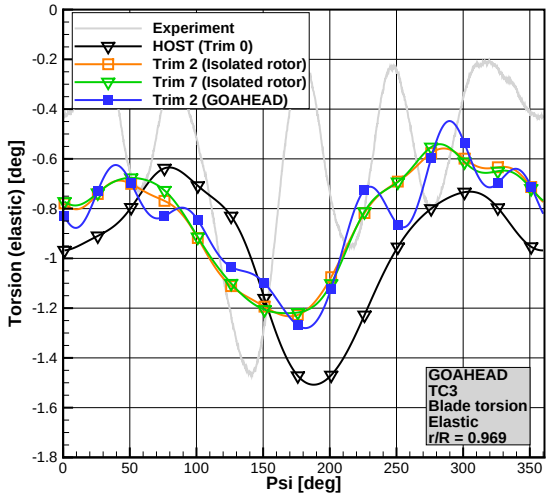

Figure 14: Computed and measured elastic torsion of the simplified GOAHEAD configuration after the second trim cycle near the blade tip. Grey curve: SPA

5 Conclusion and outlook

In the current work the newly developed toolchain for fluid-structure-trim coupling with DLRs unstructured flow solver TAU has been verified by numerical data of the validated FLOWer-HOST coupling chain. For the isolated rotor testcase all discussed numerical results are in excellent agreement among each other. Accompanying to the code-to-code verification the results have been compared to the experimental data of the GOAHEAD windtunnel campaign. The predicted blade dynamics underline the necessarity of applying fluid-structure-trim coupling for helicopter applications where CFD simulations improved accuracy compared to comprehensive rotorcodes. Still some differences to the experimental data are present which are mainly attributable to the missing interference effects. Preliminary results for a simplified GOAHEAD configuration have shown a considerable impact of the fuselage on the aerodynamics and blade dynamics. Especially the torsion and flap deflection is significantly improved. From the preliminary results it can already be concluded that the TAU-code in conjuction with the newly developed toolchain is applicable for fluid-structure-trim coupled simulation of helicopters. The valdiation of DLRs TAU-code will be continued for the simplified and the full GOAHEAD configuration.

To exploit the full advantage of the generation of mixed element meshes further work will focus on grid generation of the complex geometry of the mainrotor and tailrotorhub and the gearbox situated on the fin. The developed toolchain

is currently extended for the coupling to a newly available version of HOST which features a Python-Interface for in-memory data exchange and the possibility to perform a six-degree-of-freedom trim of a helicopter in free flight.

References

[1] B. Benoit et al. “HOST, A General Helicopter Simulation Tool for Germany and France.” In: *56th Annual Forum of the American Helicopter Society*. Virginia Beach, VA, USA, 2000.

[2] M. Biava, W. Khier, and L. Vigevano. “CFD prediction of air flow past a full helicopter configuration.” In: *Aerospace Science and Technology* 19 (2012), pp. 3–18.

[3] D.C. Wilcox. “Reassessment of the scale-determining equation for advanced turbulence models.” In: *American Institute of Aeronautics and Astronomics* 26.11 (1988), pp. 1299–1310.

[4] M. Dietz. “Simulation der Umströmung von Hubschrauberkonfigurationen unter der Berücksichtigung von Strömungs-Struktur-Kopplung und Trimmung.” PhD thesis. Universität Stuttgart: Institut für Aerodynamik und Gasdynamik, 2009.

[5] M. Dietz et al. “Numerical simulation of full helicopter configuration using weak fluid-structure coupling.” In: *46th AIAA Aerospace and Science Meeting*. Reno, NV, USA, 2008.

[6] F. De Gregorio. “Flow field characterization and interactional aerodynamic analysis of a complete helicopter.” In: *Aerospace Science and Technology* 19 (2012), pp. 19–36.

[7] C. Farhat H. Guillard. “On the Significance of the GCL for Flow Computations on Moving Meshes.” In: Proceedings of the 37th AIAA Aerospae Sciences Meeting and Exhibit. Reno, NV, USA, 1999.

[8] J. Benek and P.G. Buning and J.L. Steger. “A 3-D chimera grid embedding technique.” In: *7th Computational Fluid Dynamics Conference*. AIAA-1985-1523. Cincinatti, OH, USA, 1985.

[9] A. Jameson. “Time Dependent Calculations Using Multigrid, with Applications to Unsteady Flows Past Airfoils and Wings.” In: *AIAA 10th Computational Fluid Dynamics Conference*. AIAA Paper 91-1596. Honolulu, HI, USA, 1991.

[10] B. van der Wall K. Pahlke. “Calculation of multibladed rotors in high speed forward flight.” In: *Proceedings of the 27th European Rotorcraft Forum*. Moscow, Russia, 2001.

[11] W. Khier et al. “Trimmed CDF simulation of a complete helicopter configuration.” In: *Proceedings of the 33rd Rotorcraft Forum*. Kazaan, Russia, 2007.

[12] N. Kroll, B. Eisfeld, and H. Bleeke. *FLOWer*. Vol. 71. Notes on Numerical Fluid Mechanics. Vieweg, 1999, pp. 58–68.

[13] B. E. Launder, G. J. Reece, and W. Rodi. “Progress in the Development of a Reynolds-Stress Turbulent Closure.” In: *Journal of Fluid Mechanics* 68 (1975), pp. 537–566.

[14] K. Pahlke. “The GOAHEAD project.” In: *Proceedings of the 33rd European Rotorcraft Forum*. Kazaan, Russia, 2007.

[15] K. Pengel, R. Muller, and B.G. van der Wall. “Stereo pattern recognition - the technique for reliable rotor blade deformation and twist measurements.” In: *AHS International Meeting on Advanced Rotorcraft Technology and Life Saving Activities*. Utsunomiya Tochigi, Japan, 2002.

[16] Pointwise Inc. *Pointwise*. `http://www.pointwise.org`. 2014.

[17] P.R. Spalart and S.R. Allmaras. “A One-Equation Turbulence Model for Aerodynamic Flows.” In: *Recherche Aerospatiale* 1 (1994), pp. 5–12.

[18] D. Schwamborn, T. Gerhold, and R. Heinrich. “The DLR TAU-Code: Recent Applications in Research and Industry.” In: *Proceedings of the European Conference on Computational Fluid Dynamics ECCOMAS*. Delft, Netherlands, 2001.

[19] T. Schwarz. “Ein blockstrukturiertes Verfahren zur Simulation der Umströmung komplexer Konfigurationen.” PhD thesis. Universität Braunschweig, Germany: Institut für Aerodynamik und Strömungstechnik, 2005.

COPYRIGHT STATEMENT